Investigations of ionization-induced injection of laser wake field acceleration using phenomenological model

Qiang Chen (陈 强), Jiansheng Liu (刘建胜)*, Wentao Li (李文涛), Aihua Deng (邓爱华), Wentao Wang (王文涛), Ye Tian (田 野), and Cheng Wang (王 成)

State Key Laboratory of High Field Laser Physics, Shanghai Institute of Optics and Fine Mechanics, Chinese Academy of Sciences, Shanghai 201800, China

**Corresponding author: michaeljs_liu@mail.siom.ac.cn*

Received January 27, 2013; accepted March 3, 2013; posted online August 10, 2013

We develop a phenomenological model to investigate dynamics of ionization-induced injection. In the "bubble" regime of laser wakefield acceleration (LWFA), it is found that there is an upper limit for laser intensity of ionization-induced injection. In the plane perpendicular to the laser polarization, when the laser pulse is linearly polarized, ionization-induced injected electrons exhibit a filamented structure and semi-coherent betatron oscillation.

OCIS codes: 350.5400, 350.4990, 350.5610.
doi: 10.3788/COL201311.S23501.

Laser wakefield acceleration (LWFA)[1] concept offers more efficient path to produce high-energy electron beams (e-beams) than conventional radio frequency technology. Using the ultra-short e-beams of LWFA, it is promising to downsize kilometer-range X-ray free electron lasers to a table-top scale[2]. Experiments in 2004 demonstrated the generation of quasi-mono energetic (QM) e-beams with peak energy of near 200 MeV[3−5]. And the acceleration gradient exceeds 100 GeV/m, which is 3 orders of magnitude larger than that of the radio frequency linear accelerators. Howevera single-stage LWFA is not suitable for generating QM e-beams beyond 1 GeV because of lacking independent control on the injection and the acceleration stage[6]. And it is recognized that a two-stage LWFA[7,8] is required to obtain energy gain up to multi-GeV with a narrow energy spread.

Controlled injection of the cascaded LWFA scheme would benefit the matching between the seeding phase of the e-beams and accelerating phase of plasma waves. Tunnel-ionization-induced injection[9] is supposed to be a potential trapping mechanism for efficient injection of the e-beams into the plasma wave with lower injection threshold, more trapped charge, and lower transverse divergence. The large difference in ionization potentials between successive ionization states enables the ionization-induced injection, and electrons ionized at rest within the electron cavity gain additional energy from the net potential difference between the edge of electron cavity and its interior[10]. LWFA experiments demonstrate that intense laser pulses ionize the atoms near the peak of the laser field and accelerate e-beams up to GeV level[11]. While the accelerated e-beams exhibited large energy spread due to the continuous injection before the pump depletion of the driving laser pulse.

Generally speaking, there are three types of methods for the analysis of the wakefield generation. Hamiltonian analysis is capable of examining three-dimensional (3D) linear wakefield and one-dimensional (1D) nonlinear wakefield generation. Two/three-dimensional (2D/3D) particle-in-cell (PIC) simulations are necessary for explaining and predicting experimental LWFAs[2]. And the phenomenological method provides brief explanation of complicated phenomena and practical estimations of scaling laws. In this letter, we propose a phenomenological test particle model to investigate dynamics of ionization-induced injection. Our model assumes that the amplitudes of laser electromagnetic field and the plasma wakefield remain constant during ionization-induced injection. As theoretical and experimental results revealed, a short mixed gas length and mild density[12] (for example, 1.5×10^{18} cm^{-3}, which is much smaller than the critical density associated with 0.8-μm laser wavelength, i.e., 1.7×10^{21} cm^{-3}) of plasma is preferable for generating high-quality e-beams with large charge and low energy spread. In the plasma with such a short length and a relatively low density, ionization-induced injection takes place much earlier before self-injection of the background electrons and the driving laser pulse is far from depleted after ionization-induced injection. We neglect the influence of beam loading so that the quasi-static approximation is reasonable. And we also adopt a 'single electron' assumption, which takes into dynamics of one electron a time, simplifying the calculation, while maintaining reliability of the quasi-static approximation by avoiding beam loading inducedby mass electrons. By accumulating series of the observations of 'single electron', dynamics of ionization-induced injection can be investigated.

An intense laser pulse can expel the plasma electrons outward and create a bare ion bubble, which is suitable for accelerating and focusing the e-beams. In the high-intensity and 3D limit, the LWFA phenomena are typically observed by 3D PIC simulations. And the wakefield of the highly nonlinear bubble regime remain stable in PIC simulations through the acceleration.Theoretical works has worked out the accelerating and focusing field inside the ion cavity[2] (assumed spherical):

$$\begin{aligned} E_z &\approx (k_{\rm p}\varsigma/2)E_0, \\ E_r &\approx (k_{\rm p}r/4)E_0, \\ B_\theta &\approx -(k_{\rm p}r/4)E_0, \end{aligned} \tag{1}$$

 © 2013 Chinese Optics Letters

where E_z is the axial electric field, E_r is the radial electric field, B_θ is the azimuthal magnetic field, k_p is the plasma wave number, ς and r are the axial and radial distance away from the bubble center, respectively. Although no currently rigorous derivation is available for analysis of the matched spot size and laser profile in the bubble regime, the requirement for the matched spot size can be estimated by the rough balance between the transverse ponderomotive force of the laser and the restoring force of the ion channel, which gives $k_\mathrm{p}R \approx a_0$, where a_0 is the normalized laser amplitude and R is the radius of the bubble. While a more refined condition[6] was reformulated and presented as

$$k_\mathrm{p}R \approx k_\mathrm{p}\omega_0 = 2\sqrt{a_0}, \tag{2}$$

where ω_0 is the beam waist of the laser pulse. Equation (2) holds for $a_0 \geqslant 2$ with only slightly oscillations, and it is also found by theory and 3D PIC simulations that a spherical shape is still roughly formed for $2 \leqslant a_0 \leqslant 4$. The peak of the wakefield[6] could be estimated as

$$E_{z,\max} = \sqrt{a} m_\mathrm{e} c w_\mathrm{p}/e = \sqrt{a} E_0, \tag{3}$$

where m_e is the electronmass, e is electron charge, and E_0 is wavebreaking limit of the cold plasma.

Dynamics of the ionized electrons within the bubble is sensitive to theirinitial positions relative to the laser pulse and the wakefield. Electrons ionized at the front edge of bubble would not be trapped by the wakefield, but more inner electrons can gain more net energy from the wakefield and are more likely to be injected. The "tunneling ionization area", where the inner electrons of atoms are ionized, is determined by the laser pulse, while the "injection area" (which means that when an electron is put within the injection area at rest, it will be injected into and trapped by the wakefield) is determined by both the laser and the wakefield. The overlap of the "tunneling ionization area" and the "injection area" is the final "ionization-induced injection area", where the ionized inner electrons of atoms are just the injected electrons. Therefore, it is very important to determine the relative position between the laser pulse and the nonlinear wakefilds in the ion bubble.

However, the analytical method is difficult for the detailed analysis of the relative position in 3D nonlinear regime and currently there is no special description about this topic. Applying linearly polarized ultra-short laser pulses with the full width at half maximum (FWHM) of 30 fs, and the plasma density are all set as $n_\mathrm{e} = 1.5\times10^{18}$ cm^{-3}, we observe the 2D PIC simulations for estimations of the relative position. As shown in Fig. 1, the center of the laser pulse is approximately located near the forehead of the wakefield, for laser amplitude $a_0 = 4$ and 3. The distance is normalized to the plasma wave number, and the time is normalized to light velocity in the vacuum, and it is the same for the rest of the letter.

For both of the $a_0 = 4$ and 3 laser pulses,the bubble form are retained, and the most forehead point of the bubble is 30 fs (i.e., FWHM) ahead of the center of the laser pulses. We then analyze the ionization-induced injection of N^{5+} ions (ionized to N^{6+} ions) for both $a_0 =$ 4 and 3. The threshold for tunneling-ionization of N^{5+} ions toN^{6+} ions (ionized to N^{7+} ions) is 2.3. We scan the trajectories of series of "single electron" in the polarization plane of the laser pluses, and label the initially ionization positions of the trapped electrons as "injection area", as shown in Fig. 2.

The average tunneling ionization rate for the oscillating electric field $\overrightarrow{F}(t) = F\cos(\omega t)\overrightarrow{y}$ is

$$W = \frac{1}{\pi}\int_{-\pi/2}^{\pi/2} W_\mathrm{stat}(t)\mathrm{d}(\omega t), \tag{4}$$

where W_stat is the ionization rate for the electrostatic field with F as its amplitude

$$W_\mathrm{stat} = \frac{|B|^2}{2^{|m|}|m|!}\frac{1}{\kappa^{2Z_\mathrm{c}/\kappa-1}}\left(\frac{2\kappa^3}{F}\right)^{2Z_\mathrm{c}/\kappa-|m|-1} e^{-2\kappa^3/3F}. \tag{5}$$

We list the intermediate parameters together as

$$B = D(-1)^{(m+|m|)/2}\sqrt{\frac{(2l+1)(l+|m|)!}{2(l-|m|)!}}, \tag{6}$$

$$D = C_{n^*l}\kappa^{Z_\mathrm{c}/\kappa+1/2}, \tag{7}$$

$$C^2_{n^*l} = \left(\frac{4e^2}{n^{*2}-l^2}\right)^{n^*}\left(\frac{n^*+l}{n^*-l}\right)^{l^*+1/2}\frac{1}{2\pi n^*}, \tag{8}$$

$$\kappa = \sqrt{2I_\mathrm{p}}, \tag{9}$$

where Z_c is net charge of the ion, $n^* = Z_\mathrm{c}/\kappa$ is the effective principal quantum number, l is the orbital angular momentum quantum number, m is magnetic quantum number, and I_p is the ionization potential.

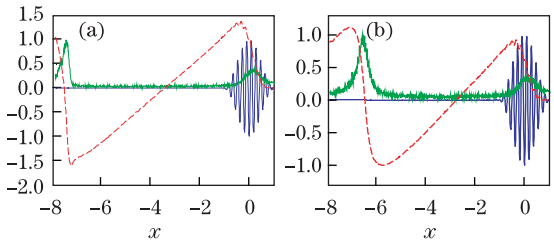

Fig. 1. (Color online) The relative position between the laser pulse and the wakefields, using 2D PIC simulations. The laser field, the axial accelerating field, and the plasma density after laser propagating 80 μm in plasma, are represented by blue solid line, red dashed line, and green dashed line. All of the peak amplitudes are all normalized to unity. (a) a_0=4; (b) a_0 = 3. The distance is normalized to the plasma wave number, and it is the same for the rest of the figures.

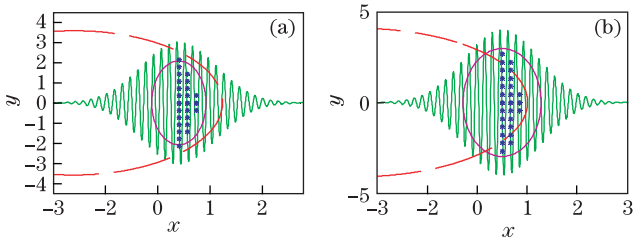

Fig. 2. (Color online) The "injection area" and the "ionization area" of (a) $a_0 = 3$ and (b) $a_0 = 4$. The "injection area" is presented by blue stars and the "ionization area" of N^{5+} ions (ionized to N^{6+}) is near the equipotential line of $a_0 =$ 2.3, represented by the purple loop.

As shown in Fig. 2(a) (the axes are rescaled for clarity) for $a_0 = 3$, the "injected electrons" in the forehead of the laser pulse is represented by stars. Here we only consider the "injected electrons" in the forehead part of the laser pulse, since the N^{6+} ions are almost totally ionized before the amplitude of the laser pulse increases to its maximum. We set $l = m = 0$, and the ionization potential of N^{5+} ions (ionized to N^{6+} ions) and N^{6+} ions (ionized to N^{7+} ions) are 552 and 667 eV, respectively. Then the calculation indicates the "ionization areas" for N^{5+} ions are just before the forehead part of purple loop ($a_0 = 2.3$), and the "injection area" for N^{6+} ions covers the forehead part within the purple loop. The "ionization-induced injection area" is the overlap of "injection area" and "ionization area". The loop crosses both the N^{5+} and N^{6+} "injection area", which indicates the existence of "ionization-induced injection area". In another word, for laser amplitude of $a_0 = 3$, the ionization-induced injection scheme works.

For the other case, $a_0 = 4$, as shown in Fig. 2(b), ionization-induced injection is impossible. N^{5+} ions are completely tunneling-ionized to N^{6+} much before a_0 reaches 2.6, which is the boundary of the injection area. Therefore, for laser amplitude of $a_0 = 4$, the ionization-induced injection of N^{5+} ions is impossible. Although the "injection area" enlarges when the amplitude of the laser pulse increase from 3, 4, the "ionization area" goes much further away from the laser pulse. As a result, no more ionization injection area exits. It is easy to conclude, with larger laser amplitude than $a_0 = 4$ (plasma density remain unchanged), the injection area would enlarge, but N^{5+} ions would be ionized more further away from the laser pulses, and the "ionization area" never cross with the "injection area".

We have revealed that in the polarization plane there is an upper limit for the laser amplitude of ionization-induced injection of N^{5+} (ionized into N^{6+}). And we can qualitatively get that, it is same for the 3D analyses of ionization-induced injection of N^{6+} (ionized into N^{7+}). More specifically, when the amplitude of the laser pulse is large enough, N^{6+} ionization happens much earlier before the laser increase to its maximum. And the ionized electrons is directly expelled by the laser pulse, rather than trapped by the wakefield. Nevertheless, more quantitative analyses, 3D PIC simulations and LWFA experiments are expected in the future for verification.

Inside the bubble, the radial focusing force is on the same level of the axial accelerating force, contributing to pull back the outward moving electrons with residual momentum. The pulling back of the relativistic injected electrons by the focusing force performs a betatron oscillation along the axis with a characteristic betatron wavelength $\lambda_\beta = (2\gamma)^{1/2}\lambda_p$, i.e., a frequency $\omega_\beta = \omega_p/(2\gamma)^{1/2}$, where γ is the Lorentz factor of the electrons. The emission of the betatron radiation is characterized by the normalized transverse momentum[13] of the oscillator $a_\beta = \gamma\beta_\perp = k_p(\gamma/2\gamma_\beta)^{1/2}$, where $\beta_\perp$ is the normalized transverse velocity, γ_β is the excursion of the oscillator. And the radiation frequency is $\omega = 2\gamma^2 N_h c k_\beta/(1+a_\beta^2/2)$, where N_h is the harmonic number and c is the light velocity in the vacuum. For $a_\beta >> 1$, the spectrum contains many harmonics with the maximum intensity occurring near the critical harmonic[2] $N_c \approx 3a_\beta^2/4$,

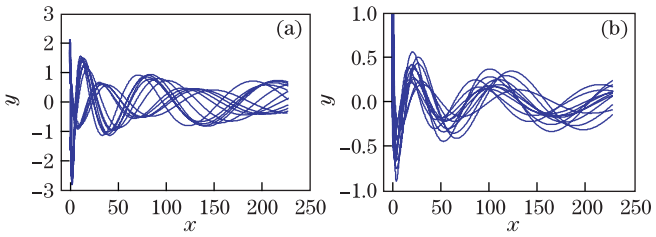

Fig. 3. (Color online) Trajectories of the ionization-induced injected electrons observed in (a) the parallel plane to the polarization of the laser pulse and (b) the perpendicular pane.

and a_β varies throughout the electron beam, from along the axis $\gamma_\beta = 0$ to the beam edge with γ_β maximized. As for the bubble regime of the LWFA, a_β can be very large, and the radiation can reach the hard X-ray regime.

Applying the phenomenological model, we choose the $a_0 = 3$ mentioned above to observe the betatron oscillations of electrons from N^{6+} ionization (ionized to N^{7+} ions). The driving laser pulse is linearly polarized, as mentioned above. The betatron oscillations are observed in the two perpendicular planes, the *s*-plane (parallel to the polarization of linearly polarized laser) and the *p*-plane (perpendicular to the polarization of linearly polarized laser), respectively. Then we also scan many ionization-induced injected electrons, assumed that ionized in 200-μm region and run for 2 mm with the accelerating wakefield. The accumulated trajectories of these electrons are shown in Fig. 3.

The trajectories of the ionized ionization injected electrons start from the region in the bubble where ionization of the electrons take place near the peak of the laser, and moves inside the bubble, as shown in Fig. 3, quite different from the trajectories of the self-injected electrons, which moves along the bubble surface and then injected in the rear the bubble. The betatron oscillations of the electrons differ between the *s*-plane and the *p*-plane. In the *s*-plane, the ionization-induced injected electrons' betatron oscillations are out of phase with each other, while in the *p*-plane, the betatron oscillations are basically in phase with each other, which is potential for the generation of semi-coherent X-ray radiation.

In conclusion, we propose a phenomenological model to investigate dynamics of ionization-induced injection of LWFA. As for bubble regime, there exists an upper limit of laser pulses amplitude for ionization-induced injection. We also investigated semi-coherent filamented structure of ionization-induced injection electrons in the plane perpendicular to the laser polarization plane,which is potential for the generation of semi-coherent X-ray radiation. We would like to anticipate that the model would enable convenient analyses of more complicated geometries using multiple pulsesor more potential schemes for ionization injection technique, as well as the generation of X-ray generation by the betatron oscillations of the ionization-induced injection electrons.

This work was supported by the National "973" Program of China (No. 2011CB808100), National Natural Science Foundation of China (Nos. 11127901, 60921004, and 10974214), Shanghai science and technology talent project (No. 12XD1405200), the State Key Laboratory Program of Chinese Ministry of Science and Technology,

and the Cooperation in the Development and Application of Femtosecond Petta-watt Level Ultra-intense and Ultra-short Laser System (No. 2011DFA11300). Finally, we would like to thank H. Xufor providing the PIC code and Shanghai Supercomputer Center.

References

1. T. Tajima and J. M. Dawson, Phys. Rev. Lett. **43,** 267 (1979).
2. E. Esarey, C. B. Schroeder, and W. P. Leemans, Rev. Mod. Phys. **81,** 1229 (2009).
3. J. Faure, Y. Glinec, A. Pukhov, S. Kiselev, S. Gordienko, E. Lefebvre, J. P. Rousseau, F. Burgy, and V. Malka, Nature **431,** 541 (2004).
4. C. G. R. Geddes, C. Toth, J. van Tilborg, E. Esarey, C. B. Schroeder, D. Bruhwiler, C. Nieter, J. Cary, and W. P. Leemans, Nature **431,** 538 (2004).
5. S. P. D. Mangles, C. D. Murphy, Z. Najmudin, A. G. R. Thomas, J. L. Collier, A. E. Dangor, E. J. Divall, P. S. Foster, J. G. Gallacher, C. J. Hooker, D. A. Jaroszynski, A. J. Langley, W. B. Mori, P. A. Norreys, F. S. Tsung, R. Viskup, B. R. Walton, and K. Krushelnick, Nature **431,** 535 (2004).
6. W. Lu, M. Tzoufras, C. Joshi, F. S. Tsung, W. B. Mori, J. Vieira, R. A. Fonseca, and L. O. Silva, Phys. Rev. STAccel. Beams **10,** 061301 (2007).
7. J. S. Liu, C. Q. Xia, W. T. Wang, H. Y. Lu, C. Wang, A. H. Deng, W. T. Li, H. Zhang, X. Y. Liang, Y. X. Leng, X. M. Lu, C. Wang, J. Z. Wang, K. Nakajima, R. X. Li, and Z. Z. Xu, Phys. Rev. Lett. **107,** 035001 (2011).
8. B. B. Pollock, C. E. Clayton, J. E. Ralph, F. Albert, A. Davidson, L. Divol, C. Filip, S. H. Glenzer, K. Herpoldt, W. Lu, K. A. Marsh, J. Meinecke, W. B. Mori, A. Pak, T. C. Rensink, J. S. Ross, J. Shaw, G. R. Tynan, C. Joshi, and D. H. Froula, Phys. Rev. Lett. **107,** 045001 (2011).
9. C. McGuffey, A. G. R. Thomas, W. Schumaker, T. Matsuoka, V. Chvykov, F. J. Dollar, G. Kalintchenko, V. Yanovsky, A. Maksimchuk, K. Krushelnick, V. Y. Bychenkov, I. V. Glazyrin, and A. V. Karpeev, Phys. Rev. Lett. **104,** 025004 (2010).
10. A. Pak, K. A. Marsh, S. F. Martins, W. Lu, W. B. Mori, and C. Joshi, Phys. Rev. Lett. **104,** 025003 (2010).
11. C. E. Clayton, J. E. Ralph, F. Albert, R. A. Fonseca, S. H. Glenzer, C. Joshi, W. Lu, K. A. Marsh, S. F. Martins, W. B. Mori, A. Pak, F. S. Tsung, B. B. Pollock, J. S. Ross, L. O. Silva, and D. H. Froula, Phys. Rev. Lett. **105,** 105003 (2010).
12. M. Chen, E. Esarey, C. B. Schroeder, C. G. R. Geddes, and W. P. Leemans, Phys. Plasmas **19,** 033101 (2012).
13. S. Cipiccia, M. R. Islam, B. Ersfeld, R. P. Shanks, E. Brunetti, G. Vieux, X. Yang, R. C. Issac, S. M. Wiggins, G. H. Welsh, M. P. Anania, D. Maneuski, R. Montgomery, G. Smith, M. Hoek, D. J. Hamilton, N. R. C. Lemos, D. Symes, P. P. Rajeev, V. O. Shea, J. M. Dias, and D. A. Jaroszynski, Nature Phys. **7,** 867 (2011).